Mechanics of Advanced Materials and Structures

ISSN: 1537-6494 (Print) 1537-6532 (Online) Journal homepage: http://www.tandfonline.com/loi/umcm20

Aerodynamic and mechanical hierarchical aeroelastic analysis of composite wings

M. Filippi & E. Carrera

To cite this article: M. Filippi & E. Carrera (2016) Aerodynamic and mechanical hierarchical aeroelastic analysis of composite wings, Mechanics of Advanced Materials and Structures, 23:9, 997-1004, DOI: 10.1080/15376494.2015.1121561

To link to this article: http://dx.doi.org/10.1080/15376494.2015.1121561

Accepted author version posted online: 08 Dec 2015.
Published online: 09 Mar 2016.

MECHANICS OF ADVANCED MATERIALS AND STRUCTURES
2016, VOL. 23, NO. 9, 997–1004
http://dx.doi.org/10.1080/15376494.2015.1121561

Taylor & Francis
Taylor & Francis Group

ORIGINAL ARTICLE

Aerodynamic and mechanical hierarchical aeroelastic analysis of composite wings

M. Filippi and E. Carrera

Department of Mechanical and Aerospace Engineering, Politecnico di Torino, Torino, Italy

ABSTRACT

The coupled bending-torsion flutter is here investigated through Carrera Unified Formulation (CUF). The hierarchical capabilities of CUF offer a procedure to obtain refined one-dimensional models that, by going beyond the assumptions of classical theories, accurately describe the kinematics of structures. Aerodynamic loadings have been determined according to Theodorsen theory, from which the steady formulation can be easily obtained. The displacement variables over the cross section (x-z plane) are approximated by x,z polynomials of any order, N. The finite element method is used to solve the governing equations, which are derived in a weak form through the principle of virtual displacements. The equations are written in terms of "fundamental nuclei," which do not vary with the theory order, N. Several wing configurations have been studied, giving great attention to thin-walled box beams made of orthotropic material. The effects of sweep angle and lamination scheme on flutter conditions have been investigated, and the results have been compared with solutions obtained from two-dimensional theories, experimental tests, and aeroelastic analyses carried out with the doublet lattice method (DLM). The unsteady theory, combined with advanced beam theories, represents a computationally cheap tool for preliminary aeroelastic studies of complex wing structures.

ARTICLE HISTORY
Received 11 November 2014
Accepted 15 November 2015

KEYWORDS
Aeroelasticity; finite element method; higher-order theories; thin-walled box; composite material; flutter

1. Introduction

Flutter is defined as the dynamic instability of an elastic body in an airstream that is subjected to large lateral aerodynamic loads. The flutter condition, which is determined by the critical speed and by a certain circular frequency, occurs when a given structure exhibits sustained, harmonic oscillations. Hence, in order to forecast borderline conditions, it is necessary to know the interactions that occur between elastic deformations and aerodynamic loads imposed by fluid motion. As far as the definition of aerodynamic loadings is concerned, many studies were presented in the first half of the 20th century by important aerodynamicists, such as Cicala [1], Ellenberger [2], Küssner [3], Burgers with von Kàrmàn [4], and, in particular, Theodorsen [5]. These strip theories, properly combined with simplified structural models, have allowed simple but reliable tools to be developed for the aeroelastic analyses.

In many papers, wings are modeled as thin-walled structures made of anisotropic materials. Even though the most reliable methodology for the study of this kind of structures is the finite element method, a number of alternative models have rapidly gained importance with the aim of limiting the computational efforts. One of the most popular of these models is the beam-plate approach, in which the bending stiffness, the torsional stiffness, and the secondary stiffnesses (bending-torsion, warping, etc.) are reduced to the beam equivalent stiffnesses (EI, GJ, K, etc.) [6]. On the basis of this methodology, aeroelastic analyses have been performed on both wing structures [7, 8] and bridge decks [9]. However, this approach is no longer considered reliable when other structural couplings, due to the distribution of the materials, may occur. For this reason, more refined theories have been developed. Over the years, Librescu et al. have treated various aspects related to fluid-structure interactions, such as the divergence conditions of swept-forward wings [10], the effects of external stores [11], and the aeroelastic tailoring of composite structures [12, 13] on both static and dynamic stability, the response to gust [14] and blast loadings [15]. In most of these papers, the wing cross section was either rectangular or biconvex, and the nonclassical effects, such as warping deformations, transverse shear, and nonuniform torsion, were included in a sophisticated beam theory. The same structural model has recently been used in [16] and [17] in which an attempt has been made to suppress the instability, and a number of interesting considerations on the different structural constitutive assumptions has been presented, respectively. In particular, since the computation of the bending and torsional stiffnesses depends on the choice of the constitutive equations, it has been pointed out, in [17], that the results of aeroelastic analyses can differ to a great extent, even as much as 40%. Moreover, other improvements have been proposed by Patil et al. in [18, 19]. The cross sectional stiffnesses of composite box beams were first computed by means of an asymptotically correct formulation and then included in a nonlinear beam modeling framework. The effectiveness of this approach has also been pointed out in [20], in which Palacios and Epureanu have dealt with the aeroelastic behavior of highly flexible wings.

It is evident that a proper description of the kinematics of complex structures is of primary importance for the prediction of the aeroelastic instability and, to this end, a simple and

CONTACT M. Filippi matteo.filippi@polito.it Department of Mechanical and Aerospace Engineering, Politecnico di Torino, Corso Duca degli Abruzzi 24. 10129, Torino, Italy.

reliable approach has been here proposed on the basis of Carrera's Unified Formulation (CUF). CUF was originally developed for plates and shells [21–23] and was later extended to the beam model [24]. This approach introduces valuable advantages especially in the study of laminated, sandwich [25], and thin-walled [26] structures. Other encouraging results have also been obtained in the rotordynamics field by analyzing both rotating blades [27] and spinning shafts [28]. As far as the structure-fluid interactions are concerned, CUF elements have already been used with both vortex [29–31] and doublet [32–34] lattice method and for supersonic flows with the piston theory [35, 36].

In the present article, for the first time, Theodorsen's aerodynamic theory has been combined with the refined beam elements for the prediction of the flutter conditions for a variety of wing configurations. With the purpose of comparison, some results related to both straight and swept plates made of either isotropic or orthotropic materials have been first compared with the solutions available in the literature. Attention was then mainly focused on thin-walled composite beam boxes characterized by nonconventional lamination schemes, for which the bending-torsion coupling can strongly affect the aeroelastic response.

2. The structural model: Carrera Unified Formulation

The CUF states that the displacement field, $\boldsymbol{u}^T(x, y, z, t) = (u_x, u_y, u_z)^T$, is an expansion of generic functions, $F_\tau(x, z)$ for the displacement vector, $\boldsymbol{u}_\tau(y)$:

$$\boldsymbol{u}(x, y, z, t) = F_\tau(x, z)\boldsymbol{u}_\tau(y, t) \qquad \tau = 1, 2, \ldots, T, \tag{1}$$

where T is the number of terms in the expansion and, according to Einstein's generalized notation, τ indicates summation. In this work, Eq. (1) consists of Taylor polynomials, which are functions of the cross section coordinates. For example, the second-order displacement field is:

$$\begin{aligned} u_x &= u_{x_1} + x\,u_{x_2} + z\,u_{x_3} + x^2\,u_{x_4} + xz\,u_{x_5} + z^2\,u_{x_6}, \\ u_y &= u_{y_1} + x\,u_{y_2} + z\,u_{y_3} + x^2\,u_{y_4} + xz\,u_{y_5} + z^2\,u_{y_6}, \\ u_z &= u_{z_1} + x\,u_{z_2} + z\,u_{z_3} + x^2\,u_{z_4} + xz\,u_{z_5} + z^2\,u_{z_6}, \end{aligned} \tag{2}$$

while the third-order displacement field becomes:

$$\begin{aligned} u_x &= u_{x_1} + x\,u_{x_2} + z\,u_{x_3} + x^2\,u_{x_4} + xz\,u_{x_5} + z^2\,u_{x_6} \\ &\quad + x^3\,u_{x_7} + x^2z\,u_{x_8} + xz^2\,u_{x_9} + z^3\,u_{x_{10}}, \\ u_y &= u_{y_1} + x\,u_{y_2} + z\,u_{y_3} + x^2\,u_{y_4} + xz\,u_{y_5} + z^2\,u_{y_6} \\ &\quad + x^3\,u_{y_7} + x^2z\,u_{y_8} + xz^2\,u_{y_9} + z^3\,u_{y_{10}}, \\ u_z &= u_{z_1} + x\,u_{z_2} + z\,u_{z_3} + x^2\,u_{z_4} + xz\,u_{z_5} + z^2\,u_{z_6} \\ &\quad + x^3\,u_{z_7} + x^2z\,u_{z_8} + xz^2\,u_{z_9} + z^3\,u_{z_{10}}. \end{aligned} \tag{3}$$

A remarkable feature is that classical beam theories can be obtained as particular cases of Taylor expansions. It should be noted that classical theories require reduced material stiffness coefficients to contrast Poisson's locking. Unless otherwise specified, Poisson locking is corrected for classical and first-order models according to Carrera and Giunta [24]. The stresses and the strains are grouped as follows:

$$\begin{aligned} \boldsymbol{\epsilon}_p &= \{\epsilon_{zz}\ \ \epsilon_{xx}\ \ \epsilon_{xz}\}^T, & \boldsymbol{\sigma}_p &= \{\sigma_{zz}\ \ \sigma_{xx}\ \ \sigma_{xz}\}^T, \\ \boldsymbol{\epsilon}_n &= \{\epsilon_{zy}\ \ \epsilon_{xy}\ \ \epsilon_{yy}\}^T, & \boldsymbol{\sigma}_n &= \{\sigma_{zy}\ \ \sigma_{xy}\ \ \sigma_{yy}\}^T, \end{aligned} \tag{4}$$

where the subscript p stands for the terms lying on the cross section, while n stands for the terms lying on the other planes, which are orthogonal to the cross section. The strain-displacement relations and Hooke's law are, respectively:

$$\begin{aligned} \boldsymbol{\epsilon}_p &= \boldsymbol{D_p}\boldsymbol{u}, \\ \boldsymbol{\epsilon}_n &= (\boldsymbol{D_{ny}} + \boldsymbol{D_{np}})\boldsymbol{u}, \end{aligned} \tag{5}$$

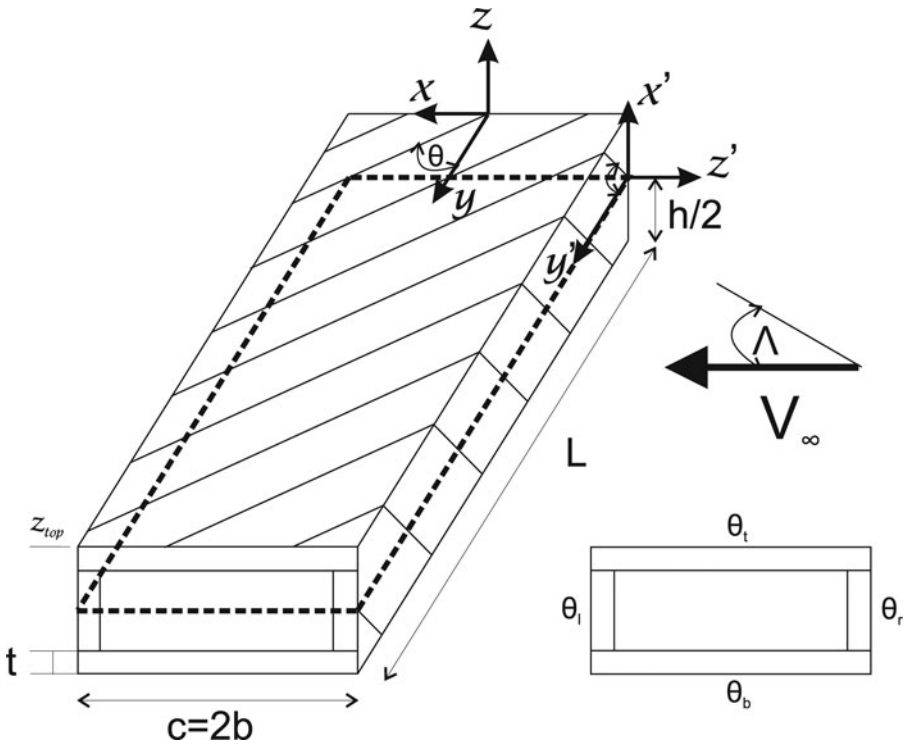

Figure 1. Sketch of the box beam and coordinate reference system.

$$\boldsymbol{\sigma}_p = \tilde{\boldsymbol{C}}_{pp}\boldsymbol{\epsilon}_p + \tilde{\boldsymbol{C}}_{pn}\boldsymbol{\epsilon}_n,$$
$$\boldsymbol{\sigma}_n = \tilde{\boldsymbol{C}}_{np}\boldsymbol{\epsilon}_p + \tilde{\boldsymbol{C}}_{nn}\boldsymbol{\epsilon}_n. \tag{6}$$

Complex laminated structures, such as box beams and cylinders, can be considered to be constituted by a certain number of either straight or curved plates of orthotropic material, whose material coordinate systems (1, 2, 3) generally do not coincide with the physical coordinate system (x, y, z) (see Figure 1). Using this approach, the matrices of the material coefficients of the generic material k are:

$$\tilde{\boldsymbol{C}}^k_{pp} = \begin{bmatrix} \tilde{C}^k_{11} & \tilde{C}^k_{12} & \tilde{C}^k_{14} \\ \tilde{C}^k_{12} & \tilde{C}^k_{22} & \tilde{C}^k_{24} \\ \tilde{C}^k_{14} & \tilde{C}^k_{24} & \tilde{C}^k_{44} \end{bmatrix}, \quad \tilde{\boldsymbol{C}}^k_{pn} = \begin{bmatrix} \tilde{C}^k_{15} & \tilde{C}^k_{16} & \tilde{C}^k_{13} \\ \tilde{C}^k_{25} & \tilde{C}^k_{26} & \tilde{C}^k_{23} \\ \tilde{C}^k_{45} & \tilde{C}^k_{46} & \tilde{C}^k_{43} \end{bmatrix},$$
$$\tilde{\boldsymbol{C}}^k_{nn} = \begin{bmatrix} \tilde{C}^k_{55} & \tilde{C}^k_{56} & \tilde{C}^k_{35} \\ \tilde{C}^k_{56} & \tilde{C}^k_{66} & \tilde{C}^k_{36} \\ \tilde{C}^k_{35} & \tilde{C}^k_{36} & \tilde{C}^k_{33} \end{bmatrix}. \tag{7}$$

For the sake of brevity, the explicit forms of the coefficients of the $\tilde{\boldsymbol{C}}$ matrices are shown in [37]. Since a classical finite element technique has here been adopted, arbitrary shaped cross sections can be handled and the generalized displacement vector becomes:

$$\mathbf{u}_\tau(y,t) = N_i(y)\mathbf{q}_{\tau i}(t), \tag{8}$$

where $N_i(y)$ are the shape functions and $\mathbf{q}_{\tau i}(t)$ is the nodal displacement vector:

$$\mathbf{q}_{\tau i}(t) = \left\{ q_{u_{x_{\tau i}}} \quad q_{u_{y_{\tau i}}} \quad q_{u_{z_{\tau i}}} \right\}^T. \tag{9}$$

3. 2D steady and unsteady aerodynamic theories

Theodorsen was the first to propose a complete solution for a thin airfoil that undergoes harmonic lateral oscillations in an incompressible fluid. Adopting the assumptions of the small-disturbance theory, Theodorsen considered a flat plate with a control surface, which could move in vertical translation $h(t)$ and rotate about an axis at $x = ba$ through an angle $\alpha(t)$. The final expression of the lift, due to both translation and rotation as derived in [38], is:

$$L = \pi\rho_a b^2[\ddot{h} + U\dot{\alpha} - ba\ddot{\alpha}] + 2\pi\rho_a U b C(k)\left[\dot{h} + U\alpha + b\left(\frac{1}{2} - a\right)\dot{\alpha}\right], \tag{10}$$

where U is the free-stream velocity, b the semichord, ρ_a the air density and $C(k)$ the deficiency lift function, which depends on the so-called *reduced frequency* $k = \frac{\omega U}{b}$. a defines the position of the rotation axis with respect to the center of the section and it is dependent on the support condition, the lamination scheme, and the applied load. Owing to the difficulty involved in defining its correct value for swept and asymmetric laminated structures, the elastic offset a is assumed to be null. Theodorsen identified the term $C(k)$ as a Hankel function of the second kind, which is, in turn, comprised of Bessel functions of the first and second kinds [38, 39]:

$$C(k) = F(k) + iG(k) = \frac{H^{(2)}_1(k)}{H^{(2)}_1(k) + iH^{(2)}_0(k)}. \tag{11}$$

A simplified expression of Theodorsen's function was proposed by R.T. Jones [40], who presented an exponential approximation of Wagner's indicial solution (1925):

$$C(k) \approxeq 1 - \frac{0.165}{1 - (0.0455/k)i} - \frac{0.335}{1 - (0.3/k)i}. \tag{12}$$

The first contribution in Eq. (10), contains the virtual mass (or noncirculatory) terms that act as a form of inertia of the fluid surrounding the airfoil and, since the single and doubly-differentiated terms relative to the mass properties of the structure are small, they are usually neglected. The remaining terms determine the value of the lift and represent the circulatory part. The steady-state simplification can be easily obtained by replacing the function $C(k)$ with the unitary value and omitting the term containing $\dot{\alpha}$:

$$L \approxeq 2\pi\rho_a U b[\dot{h} + U\alpha]. \tag{13}$$

For the special purpose of correcting the sectional lift coefficient C_L relating to the influence of the aspect ratio ($\mathrm{AR} = \frac{2L_w}{c_m}$) and the sweep angle ($\Lambda$), Diederich's approximation is used:

$$c_{l\alpha} = \frac{dC_L}{d\alpha} = \frac{\pi\ AR}{\pi\ AR\ + c_{l\alpha 0}\cos(\Lambda)}\ c_{l\alpha 0}\ \cos(\Lambda), \tag{14}$$

where L_w is the length of the wing, c is the mean chord (see Figure 1), and $c_{l\alpha 0}$ is the lift-curve slope, which is equal to 2π. Finally, since the quantity $b\pi$ may be approximated with the integral $\int_{-b}^{b}\sqrt{\frac{b-x}{b+x}}dx$, which is able to reproduce the distribution of pressure over a slightly inclined, thin, and uncambered airfoil, Eqs. (10) and (13) become, respectively,

$$L = \frac{2\pi\ AR\ \cos(\Lambda)}{\pi\ AR\ + 2\pi\cos(\Lambda)}\int_{-b}^{b}\sqrt{\frac{b-x}{b+x}}dx\ \rho_a U C(k) \times\left[\dot{h} + U\alpha + b\left(\frac{1}{2} - a\right)\dot{\alpha}\right], \tag{15}$$

$$L \approxeq \frac{2\pi\ AR\ \cos(\Lambda)}{\pi\ AR\ + 2\pi\cos(\Lambda)}\int_{-b}^{b}\sqrt{\frac{b-x}{b+x}}dx\ \rho_a U[\dot{h} + U\alpha]. \tag{16}$$

4. The equations of motion in the CUF framework

The equations of motion of a generic structure oscillating in an incompressible flow can be derived directly by means of the principle of virtual displacement, which states:

$$\delta L_{int} = \delta L_{ext} + \delta L_{ine}, \tag{17}$$

where L_{int} and L_{ine} are the strain energy and the inertial loading work, respectively, whereas L_{ext} is the contribution of the external loadings and δ stands for virtual variation.

4.1. Strain energy

The virtual variation of the strain energy can be written using Eqs. (1), (5), (6), and (8) in compact format

$$\delta L_{int} = \delta {q_{\tau i}}^T \boldsymbol{K}^{ij\tau s} q_{si}, \tag{18}$$

where $\boldsymbol{K}^{ij\tau s}$ is the stiffness matrix in the form of the fundamental nucleus, and which, in compact notation, can be written as follows:

$$\begin{aligned}\boldsymbol{K}^{ij\tau s} = {} & I_l^{ij} \lhd \boldsymbol{D}_{np}^T(F_\tau \boldsymbol{I}) \left[\tilde{\boldsymbol{C}}_{np}^k \boldsymbol{D}_p(F_s \boldsymbol{I}) + \tilde{\boldsymbol{C}}_{nn}^k \boldsymbol{D}_{np}(F_s \boldsymbol{I})\right] \\ & + \boldsymbol{D}_p^T(F_\tau \boldsymbol{I}) \left[\tilde{\boldsymbol{C}}_{pp}^k \boldsymbol{D}_p(F_s \boldsymbol{I}) + \tilde{\boldsymbol{C}}_{pn}^k \boldsymbol{D}_{np}(F_s \boldsymbol{I})\right] \rhd \\ & + I_l^{ij,y} \lhd \left[\boldsymbol{D}_{np}^T(F_\tau \boldsymbol{I}) + \boldsymbol{D}_p^T(F_\tau \boldsymbol{I}) \tilde{\boldsymbol{C}}_{pn}^k\right] F_s \rhd + \boldsymbol{I}_{Ay} \\ & + I_l^{i,yj} \boldsymbol{I}_{Ay}^T \lhd F_\tau \left[\tilde{\boldsymbol{C}}_{np}^k \boldsymbol{D}_p(F_s \boldsymbol{I}) + \tilde{\boldsymbol{C}}_{nn}^k \boldsymbol{D}_{np}(F_s \boldsymbol{I})\right] \rhd \\ & + I_l^{i,yj,y} \boldsymbol{I}_{Ay}^T \boldsymbol{I}_{Ay} \lhd F_\tau \tilde{\boldsymbol{C}}_{nn}^k F_s \rhd,\end{aligned} \tag{19}$$

where

$$\boldsymbol{I}_{Ay} = \begin{bmatrix} 0 & 0 & 1 \\ 1 & 0 & 0 \\ 0 & 1 & 0 \end{bmatrix}, \qquad \lhd \ldots \rhd = \int \ldots dA, \tag{20}$$

$$\begin{aligned}&\left(I_l^{ij},\ I_l^{ij,y},\ I_l^{i,yj},\ I_l^{i,yj,y},\ I_l^{i}\right) \\ &\quad = \int_l \left(N_i N_j,\ N_i N_{j,y},\ N_{i,y} N_j,\ N_{i,y} N_{j,y},\ N_i\right) dy.\end{aligned} \tag{21}$$

Apex k indicates the layer, and the material is therefore not considered constant in the integral over cross section A. This allows composite structures and nonhomogeneous sections to be investigated.

4.2. Kinetic energy

Similarly, the virtual work of inertial loads L_{ine} for a composite structure becomes:

$$\delta L_{ine} = \delta \boldsymbol{q}_{\tau i}^T \boldsymbol{M}^{ij\tau s} \ddot{\boldsymbol{q}}_{sj}\, dy, \tag{22}$$

where $\ddot{\boldsymbol{q}}$ is the nodal acceleration vector and $\boldsymbol{M}^{ij\tau s}$ is the mass matrix in the form of the fundamental nucleus:

$$\boldsymbol{M}^{ij\tau s} = I_l^{ij} \lhd (F_\tau \rho^k \boldsymbol{I} F_s) \rhd . \tag{23}$$

4.3. External work

The work due to the lift can generally be written as:

$$\delta L_{ext} = \int_y \int_x \delta u_z(x, y, z_{top})\, L(x, y, z_{top})\, dx\, dy, \tag{24}$$

where z_{top} is the upper z-coordinate of the cross section. Equation (24) with Eq. (10), becomes:

$$\begin{aligned}\delta L_{ext} = cost \Bigg[& \int_y \int_x \delta \boldsymbol{u}^T \sqrt{\frac{b-x}{b+x}}\, I_L\, \dot{\boldsymbol{u}} + \delta \boldsymbol{u}^T \sqrt{\frac{b-x}{b+x}}\, I_L\, \boldsymbol{u}_{,x} \\ & + \delta \boldsymbol{u}^T\, b \left(\frac{1}{2} - a\right) \sqrt{\frac{b-x}{b+x}}\, I_L\, \dot{\boldsymbol{u}}_{,x} \Bigg]\, dx\, dy,\end{aligned} \tag{25}$$

where it has been assumed that:

$$\dot{h} = \dot{u}_z, \qquad \alpha = \frac{du_z}{dx} = u_{z,x}, \qquad \dot{\alpha} = \dot{u}_{z,x},$$

and

$$\boldsymbol{I}_L = \begin{bmatrix} 0 & 0 & 0 \\ 0 & 0 & 0 \\ 0 & 0 & 1 \end{bmatrix}, \qquad cost = \frac{2\pi\, AR\, \cos(\Lambda)}{\pi\, AR + 2\pi\, \cos(\Lambda)}\, \rho_a\, U\, C(k).$$

By introducing Eqs. (1) and (8) into Eq. (25), we obtain:

$$\delta L_{ext} = \delta \boldsymbol{q}_{\tau i}^T \boldsymbol{D}_L^{ij\tau s} \dot{\boldsymbol{q}}_{sj} + \delta \boldsymbol{q}_{\tau i}^T \boldsymbol{K}_L^{ij\tau s} \boldsymbol{q}_{sj} + \delta \boldsymbol{q}_{\tau i}^T \boldsymbol{D}_{Lm}^{ij\tau s} \dot{\boldsymbol{q}}_{sj}, \tag{26}$$

where $\boldsymbol{D}_L^{ij\tau s}$, $\boldsymbol{K}_L^{ij\tau s}$, $\boldsymbol{D}_{Lm}^{ij\tau s}$, and $\boldsymbol{F}_L^{i\tau}$ are the aerodynamic contributions. The first and the third matrices introduce damping into the system, whereas the third matrix represents the aerodynamic stiffness. The last term is a forcing vector that can be overlooked in free-vibration analyses. The aforementioned matrices, written in terms of fundamental nuclei, result to be:

$$\begin{aligned}\boldsymbol{D}_L^{ij\tau s} &= cost\, I_l^{ij} \lhd \left(\sqrt{\frac{b-x}{b+x}} F_\tau(x, z_{top}) \boldsymbol{I}_L F_s(x, z_{top})\right) \rhd_x, \\ \boldsymbol{K}_L^{ij\tau s} &= cost\, I_l^{ij} \lhd \left(\sqrt{\frac{b-x}{b+x}} F_{\tau,x}(x, z_{top}) \boldsymbol{I}_L F_s(x, z_{top})\right) \rhd_x, \\ \lhd \ldots \rhd_x &= \int_{-b}^{b} \ldots dx, \\ \boldsymbol{D}_{Lm}^{ij\tau s} &= cost\, I_l^{ij}\, b \left(\frac{1}{2} - a\right) \lhd \left(\sqrt{\frac{b-x}{b+x}} F_{\tau,x}(x, z_{top}) \boldsymbol{I}_L F_s(x, z_{top})\right) \rhd_x .\end{aligned} \tag{27}$$

The quadratic eigenvalue problem (QEP) of generic order R assuming a periodic solution $\boldsymbol{q} = \bar{\boldsymbol{q}} e^{i\omega t}$ to solve the equations of motion (EoM), is transformed into a classical linear system of $2{\times}R$ order:

$$\begin{cases} \boldsymbol{M}\ddot{\boldsymbol{q}} + (\boldsymbol{D}_L + \boldsymbol{D}_{Lm})\dot{\boldsymbol{q}} + (\boldsymbol{K} + \boldsymbol{K}_L)\, \boldsymbol{q} = 0 \\ -\dot{\boldsymbol{q}} + \dot{\boldsymbol{q}} = 0 \end{cases}, \tag{28}$$

and by introducing:

$$\boldsymbol{a} = \begin{Bmatrix} \boldsymbol{q} \\ \dot{\boldsymbol{q}} \end{Bmatrix} \qquad \dot{\boldsymbol{a}} = \begin{Bmatrix} \dot{\boldsymbol{q}} \\ \ddot{\boldsymbol{q}} \end{Bmatrix}, \tag{29}$$

the equations of motion assume the following form:

$$\frac{\boldsymbol{R}}{\boldsymbol{T}} - \frac{1}{i\omega} \boldsymbol{I} = 0, \tag{30}$$

where

$$\boldsymbol{T}^{-1}\boldsymbol{R} = \begin{bmatrix} (\boldsymbol{K} + \boldsymbol{K}_L)^{-1}(\boldsymbol{D}_L + \boldsymbol{D}_{Lm}) & (\boldsymbol{K} + \boldsymbol{K}_L)^{-1}\boldsymbol{M} \\ -\boldsymbol{I} & \boldsymbol{0} \end{bmatrix}. \tag{31}$$

Since the aerodynamic matrices depend on the reduced frequency k, the solutions are found by means of an iterative procedure. The frequencies are introduced by trial and error for any speed in the considered range, until Eq. (30) is obtained. The flutter velocity is determined when the real part of one eigenvalue is null.

Table 1. Flutter conditions for an isotropic plate.

	ST		TM		DLM [40]	
	V_F	f_F	V_F	f_F	V_F	f_F
TE2	(50.2)	(45.000)	(60.6)	(36.823)	—	—
	56.1	45.435	67.6	35.945	69.4	40.002
TE3	(49.5)	(42.904)	(59.5)	(35.257)	—	—
	55.6	43.622	66.2	34.363	68.5	39.029
TE4	(49.8)	(43.395)	(59.5)	(35.244)	—	—
	55.6	43.607	66.2	34.350	68.4	38.995

(): the lift coefficient is not corrected.

5. Numerical results

A cantilever straight plate was considered in the first numerical example. The length (L), the thickness (t), and the width (c) of the investigated model were 0.305, 0.0762, and 0.001 m, respectively. The material, whose properties were $E = 73.8$ GPa, $\nu = 0.3$, and $\rho = 2768$ Kg/m^3, was isotropic. Both flutter velocity [m/s] and frequency [Hz] were computed using both the steady (ST) and unsteady (TM) models with different displacement expansions. These results are reported in Table 1 and compared with those found in [41], where the doublet lattice method (DLM) was combined with Carrera's Unified Formulation. In this case, the use of the second-order Taylor-like expansion guarantees acceptable results with a very low number of degrees of freedom. It should be noted that, with the corrected lift coefficient, the flutter velocities (V_F) computed with the TM are very close to the reference values while, with the ST, they are generally lower. However, the steady theory provided higher values of the flutter frequencies, especially with respect to those computed using Theodorsen's model. The effects of the sweep angle (Λ) were then investigated for the same structure. The ST and TM results are compared in Table 2 with those presented in [34], in which the dynamic stiffness method (DSM) was combined with the DLM in the CUF framework. The analyses of the swept configurations have required the use of more refined displacement theories in order to describe the bending-torsional coupling properly. For this reason, the third-order theory (TE3) was necessary to ensure convergence of the results. A positive angle of sweep implies a decrease in the flutter conditions. The steady theory again predicted lower flutter velocities and higher frequencies than the TM and DLM, which have yielded similar velocity values.

Table 2. Flutter conditions for an isotropic plate.

		V_F [m/s]			f_F [Hz]		
Λ	Theory	TE2	TE3	TE4	TE2	TE3	TE4
0°	ST	56.086	55.595	55.589	45.435	43.607	43.622
	TM	67.564	66.247	66.231	35.945	34.363	34.350
	DLM [34]	69.388	68.503	68.523	40.002	39.029	38.995
10°	ST	55.949	54.630	54.609	41.602	40.774	40.708
	TM	64.270	63.019	62.986	32.912	32.193	32.155
	DLM [34]	65.441	64.305	64.506	38.362	37.361	37.352
20°	ST	58.665	53.853	53.721	38.914	37.791	37.635
	TM	64.845	60.352	60.210	31.223	29.859	29.770
	DLM [34]	66.408	61.046	59.130	36.736	35.095	34.793
30°	ST	63.627	53.147	52.714	35.803	33.977	33.750
	TM	68.397	57.938	57.514	29.885	27.108	26.864
	DLM [34]	70.145	57.747	57.216	34.156	31.887	31.616

Table 3. Flutter condition for a six-layer plate $[30_2/0]_S$.

	ST		TM		DLM [42]	
	V_F	f_F	V_F	f_F	V_F	f_F
TE2	25.969	27.185	28.726	23.132	28.820	27.813
TE3	24.007	26.318	26.696	22.142	25.938	26.651
TE4	23.915	26.216	26.590	22.038	25.937	26.650

Table 4. Flutter velocities for a six-layer plate, TE3.

Lamination	ST	TM	CLT [43]	EXP [44]	DLM [42]
$[0_2/90]_S$	19.2	23.5	23.0	25	23.2
$[45/-45/0]_S$	40.1	44.2	40.1	>32	40.3
$[45_2/0]_S$	25.0	27.8	27.5	28	26.2
$[30_2/0]_S$	24.0	26.7	27.1	27	25.9

Other analyses were carried out on straight and swept composite plates. A six-layer cantilevered beam was first considered. The dimension L remained equal to that of the previous structures, while the total thickness and the width were assumed to be 0.804 and 76.2 mm, respectively. The properties of the orthotropic material were $E_L = 98$ [GPa], $E_T = 7.90$ [GPa], $G_{LT} = 5.60$ [GPa], $\nu = 0.28$, and $\rho = 1520$ [kg/m^3]. The flutter conditions for the stacking sequence $[30_2/0]_S$ are compared in Table 3 with those predicted by the DLM [42], using three different displacement theories. Despite the discrepancies between the flutter frequencies, the three aerodynamic approaches again predicted similar flutter velocities for this case. This is also confirmed in Table 4 where, for different lamination schemes, the flutter velocities computed using the TE3 displacement model are compared with 2D (CLT) and experimental (EXP) solutions. The influence of the lamination scheme on the flutter conditions has also been evaluated considering the $[\theta_2/90_2^\circ/-\theta_2]$ configuration. Figure 2 shows the instability velocities computed

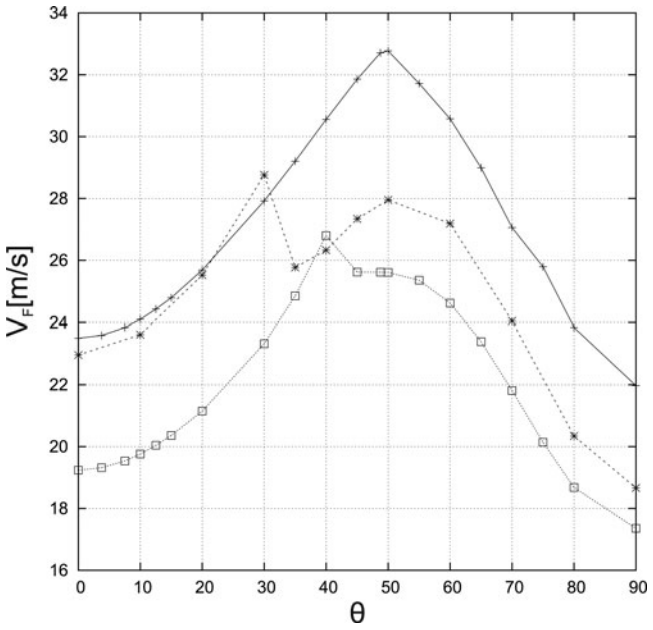

Figure 2. Flutter velocities on the angle ply for the lamination case $[\theta_2/90_2{}^\circ/-\theta_2]$: $-\star-$: DLM, $-+-$: TM, $-\square-$: ST.

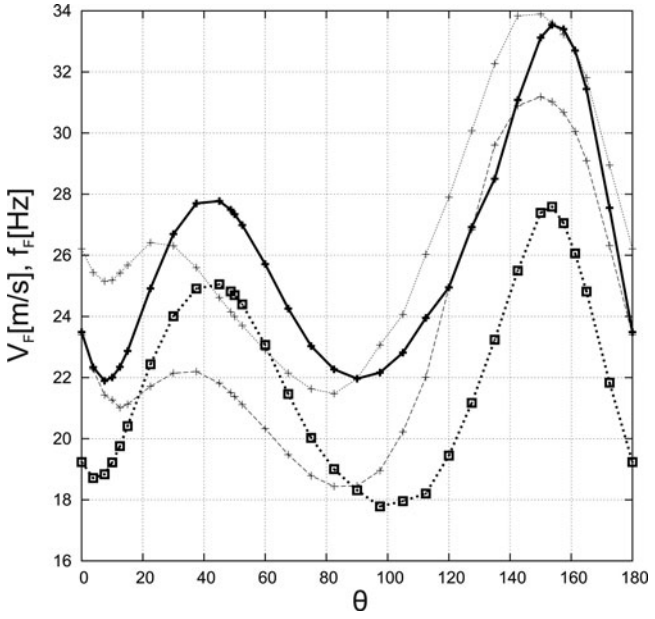

Figure 3. Flutter velocities (bold lines) and frequencies (lines) on the angle ply for the lamination case $[\theta/\theta/0^\circ]_S$: $-+-$: TM, $-\square-$: ST.

with the TE3 displacement model as a function of the angle-ply θ. Even though the steady approach yielded more conservative results, it should be noted that the strip theories predict similar variations of the flutter speeds, which have reached maximum values between of 40° and 50°. Instead, when the DLM is adopted, the flutter speed initially increases with the angle, and then rapidly decreases when θ is equal to 35°. After this drop, the DLM results fall between those of the two strip theories. Figure 3 also shows both the frequencies and velocities of flutter computed with the steady and unsteady strip theories for the symmetric lamination schemes $[\theta/\theta/0^\circ/]_S$ as a function of the lamination angle. Again the theories qualitatively yielded the same variations for these configurations, which involve bending-torsional coupling, and predict maximum values of the velocities and frequencies for $150^\circ < \theta < 160^\circ$.

A symmetric eight-layer lamination was adopted for the beam configuration. The total thickness of the laminate is equal to 0.804 mm; the stacking sequence is $[22.5/67.5/22.5/67.5]_S$, and the thicknesses of the plies are 0.03678, 0.04824, 0.06432, and 0.25326 mm, respectively. The natural frequencies (bending and torsion), flutter conditions, and the results from the CLT model are presented in Table 5. The above considerations are also valid for this case.

Table 5. Flutter velocities [m/s] for an eight-layer plate, TE3.

	f_1	f_2	f_3	f_4	f_5	V_F
			$\Lambda = 0^\circ$			
ST	7.2	45.1	59.1	126.5	182.5	30.7
TM	7.2	45.1	59.1	126.5	182.5	36.5
DLM [42]	7.2	45.1	58.9	126.5	181.9	38.2
CLT [43]	7.3	45.4	59.1	127.7	182.3	38.8
			$\Lambda = 30^\circ$			
ST	5.6	34.5	59.9	96.2	187.5	29.5
TM	5.6	34.5	59.9	96.2	187.5	32.9
DLM [42]	5.6	34.4	59.6	95.9	182.7	32.0
CLT [43]	5.6	34.4	60.0	95.4	182.0	32.4

Table 6. Material properties and dimensions of the composite box beam shown in Figure 1.

Property	Dimension
E_{11}	206.8 [Gpa]
E_{22}	5.17 [Gpa]
G_{23}	2.55 [Gpa]
G_{31}	2.55 [Gpa]
G_{12}	3.10 [Gpa]
ν_{12}	0.25
ρ	1528.5 [kg/m^3]
c	0.5 [m]
h	c/15 [m]
t	c/150 [m]
L	3.5 [m]

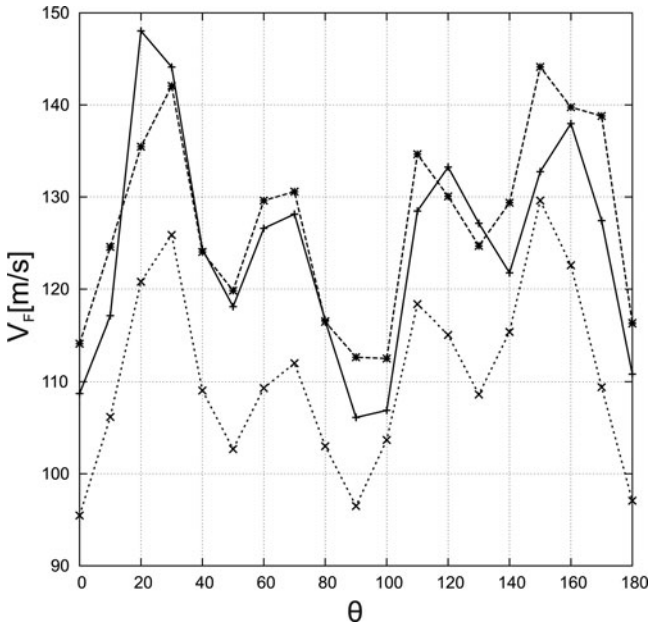

Figure 4. Flutter velocities on the angle ply of the box beam: $-\star-$: DLM, $-+-$: TM, $-\times-$: ST.

As previously mentioned, since the wing was modeled as a box structure in a number of studies, a prismatic thin-walled beam was considered. The structure was discretized with seven 4-node beam-elements and its dimensions and material properties are listed in Table 6. According to the $[\theta_b/\theta_r/\theta_t/\theta_l]$ configuration of Figure 1 and in order to consider an arbitrary lamination sequence in which the bending-torsion coupling may occur, the $[\theta/0.1\theta/2\theta/10\theta]$ case was considered. Adopting the fourth-order Taylor-like expansion (TE4), the flutter velocities were computed with the three above approaches and their changes, as a function of the angle ply, are shown in Figure 4. It should be noted that the accuracy of the unsteady strip theory, with respect to the panel method, can be considered acceptable, since the maximum relative difference is about 10%, while the

Table 7. Flutter velocities [m/s] for the angle ply box beam, TE4.

	0°	30°	60°	90°	120°	150°	180°
ST	95.462	125.88	109.30	96.492	115.08	129.61	97.07
TM	108.71	144.12	126.59	106.11	133.24	132.75	110.82
DLM	114.12	142.06	129.62	112.66	130.07	144.14	116.32

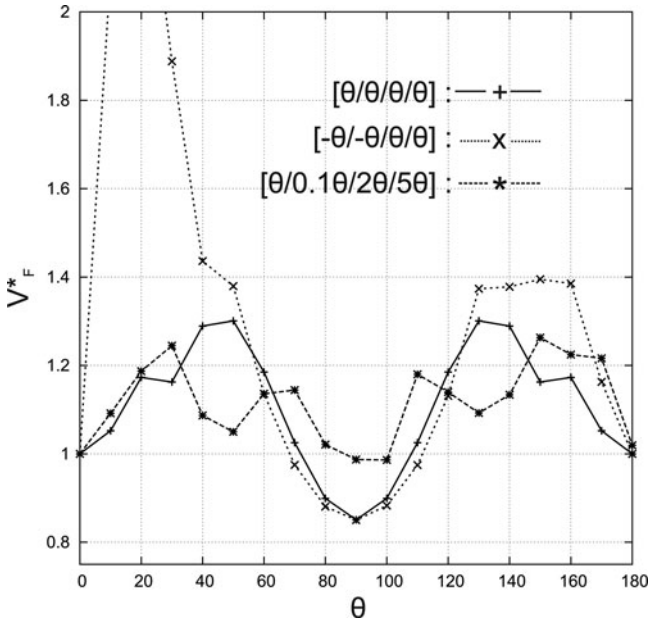

Figure 5. Normalized flutter velocities V^*_F on the angle ply of the box beam for three different lamination schemes (DLM).

steady aerodynamic theory has always yielded lower speed values. Moreover, Table 7 shows the flutter velocities for a number of angle values.

Although it has been proved that the unsteady strip theory in the CUF framework provides good results for a number of structures, panel methods are more reliable approaches for the aeroelastic design of composite thin-walled structures. For this reason, other analyses were carried out on the previous box structure, using the DLM, in order to compare different lamination schemes. The results shown in Figure 5 are normalized with respect to the flutter speed, when θ is equal to 0°. As expected, the solution related to the first scheme $[\theta/\theta/\theta/\theta]$ is symmetric with respect to the minimum flutter speed, which occurs for θ equal to 90°. The two maximum speed values are reached for θ equal to 50° and 130°. Although the worst condition is the same as that of the previous configuration, the second scheme $[-\theta/-\theta/\theta/\theta]$) provides the highest flutter speed for the considered cases, when θ is equal to 20°. Finally, as far as the last case $[\theta/0.1\,\theta/2\,\theta/10\,\theta]$ is concerned, maximum value (at $\theta = 150°$) is lower than those of the previous examples, but it is interesting to note that, with this configuration, the minimum speed is the highest (at $\theta = 90°$).

6. Conclusion

One-dimensional finite elements based on various displacement fields have been used in this article to perform aeroelastic analyses of straight and swept, compact, and thin-walled beams made of isotropic and composite materials. Both structural and aerodynamic models have been obtained considering the Carrera Unified Formulation. The flutter conditions obtained with the steady and unsteady strip theories, for the first time developed on the basis of CUF, have been compared with both theoretical and experimental results available in the literature as well as with those obtained with the DLM. In light of these results, it is possible to draw the following conclusions:

- Since the flutter phenomenon involves a bending-torsion coupling, refined beam models are needed to predict an accurate dynamic response of the structure;
- While the steady approach predicts too low flutter velocity values, the unsteady strip theory generally yields results very close to the reference values;
- As expected, the lamination scheme and the sweep angle affect the dynamics of the structures to a great extent. Therefore, the setting of these two parameters is crucial for a correct aeroelastic design.

Further investigations could be addressed to the aeroelastic studies of complex wing configurations, such as thin-walled boxes with transversal and longitudinal stiffeners. Furthermore, although the unsteady strip theory introduces important approximations, it can be considered a good tool for the preliminary aeroelastic analyses of rotating blades made of either composite or isotropic materials.

References

[1] P. Cicala, Le azioni aerodinamiche sui profili di ala oscillanti in presenza di corrente uniforme, Mem. R. Accad. Sci. Torino, vol. 70, pp. 356–371, 1934–1935.
[2] G. Ellenberger, Bestimmung der luftkräfte auf einen ebenen tragflügel mit querruder, Z. Angew. Math. Mech., vol. 16, p. 199, 1936.
[3] H.G. Küssner, Zusammenfassender berichtüber den instationären auftrieb von flügeln, Luftfahrt-Forschung, vol. 13, pp. 410–424, 1936.
[4] T. von Kàrmàn and J.M. Burgers, General aerodynamic theory of perfect fluids. In: Aerodynamic Theory (Vol. II), W.F. Durand, Ed., Dover, New York, 1943 (originally published in 1934).
[5] T. Theodorsen, General theory of aerodynamic instability and the mechanisms of flutter, N.A.C.A. Report 496, 1935.
[6] Z. Qin and L. Librescu, Flutter and divergence aeroelastic characteristics for composite forward swept cantilevered wing, J. Aircr., vol. 22, pp. 1001–1007, 1985.
[7] S.J. Guo, J.R. Banerjee, and C.W. Cheung, The effect of laminate layup on the flutter speed of composite wings, J. Aerosp. Eng., vol. 217, pp. 115–122, 2003.
[8] S.J. Guo, W. Cheng, and C. Degang, Aeroelastic tailoring of composite wing structures by laminate layup optimization. Technical notes, AIAA J., vol. 44, pp. 3146–3149, 2006.
[9] J.R. Banerjee, A simplified method for the free vibration and flutter analysis of bridge decks, J. Sound Vib., vol. 260, pp. 829–845, 2003.
[10] L. Librescu and A. Khdeir, Aeroelastic divergence of swept-forward composite wings including warping restraint effect, AIAA J., vol. 26, pp. 1373–1377, 1988.
[11] F. Gem and L. Librescu, Static and dynamic aeroelasticity of advanced aircraft wings carrying external stores, AIAA J., vol. 36, pp. 1121–1129, 1998.
[12] F. Gem and L. Librescu, Aeroelastic tailoring of composite wings exhibiting nonclassical effects and carrying external stores, J. Aircr., vol. 37, pp. 1097–1104, 2000.
[13] Z. Qin and L. Librescu, Aeroelastic instability of aircraft wings modelled as anisotropic composite thin-walled beams in incompressible flow, J. Fluids Struct., vol. 18, pp. 43–61, 2003.
[14] Z. Qin, L. Librescu, and P. Marzocca, Aeroelastic instability and response of advanced aircraft wings at subsonic flight speeds, Aerosp. Sci. Technol., vol. 6, pp. 195–208, 2002.
[15] P. Marzocca, L. Librescu, and G. Chiocchia, Aeroelastic response of a 2-D airfoil in a compressible flow field and exposed to blast loading, Aerosp. Sci. Technol., vol. 6, pp. 259–272, 2002.
[16] S. Ji-Seok, C. Jeonghwan, C. Seog-Ju, N. Sungsoo, and Z. Qin, Robust aeroelastic instability suppression of an advanced wing with model uncertainty in subsonic compressible flow field, Aerosp. Sci. Technol., vol. 25, pp. 242–252, 2013.

[17] P.K. Masjedi and H.R. Ovesy, Aeroelastic instability of composite wings by the consideration of different structural constitutive assumptions, J. Fluids Struct., vol. 49, pp. 303–321, 2014.
[18] C.E.S. Cesnik, D.H. Hodges, and M.J. Patil, Aeroelastic analysis of composite wings. Proceedings of the 37th Structures, Structural Dynamics and Materials Conference, April 15–17, Salt Lake City, Utah, 1996.
[19] M.J. Patil, Aeroelastic tailoring of composite box beams, Proceedings of the 35th Aerospace Sciences Meeting and Exhibit, January 6–9, Reno, Nevada, 1997.
[20] R. Palacios and B.I. Epureanu, An intrinsic description of the nonlinear aeroelasticity of very flexible wings, Proceedings of the 52nd AIAA/ASME/ASCE/AHS/ASC Structures, Structural Dynamics and Materials Conference, April 4–7, Denver, Colorado, 2011.
[21] E. Carrera, Theories and finite elements for multilayered, anisotropic, composite plates and shells, Arch. Comput. Methods Eng., vol. 9, no. 2, pp. 87–140, 2002.
[22] E. Carrera, Theories and finite elements for multilayered plates and shells: A unified compact formulation with numerical assessment and benchmarking, Arch. Comput. Methods Eng., vol. 10, no. 3, pp. 216–296, 2003.
[23] E. Carrera, Assessment of theories for free vibration analysis of homogeneous and multilayered plates, Shock Vib., vol. 3–4, pp. 261–270, 2004.
[24] E. Carrera, G. Giunta, and M. Petrolo, Beam Structures: Classical and Advanced Theories, John Wiley and Sons, Inc., Chichester, UK, 2011.
[25] E. Carrera, M. Filippi, and E. Zappino, Laminated beam analysis by polynomial, trigonometric, exponential and zig-zag theories, Eur. J. Mech. A, Solids, vol. 41, pp. 58–69.
[26] E. Carrera, M. Filippi, and E. Zappino, Free vibration analysis of laminated beam by polynomial, trigonometric, exponential and zig-zag theories, J. Compos. Mater., vol. 48, pp. 2299–2316, 2013.
[27] E. Carrera, M. Filippi, and E. Zappino, Free vibration analysis of rotating composite blades via Carrera unified formulation, Compos. Struct., vol. 106, pp. 317–325, 2013. DOI: 10.1016/j.compstruct.2013.05.055.
[28] E. Carrera, M. Filippi, and E. Zappino, Analysis of rotor dynamic by one-dimensional variable kinematic theories, J. Eng. Gas Turbines Power, vol. 135, art. 092501, 2013. DOI: 10.1115/1.4024381.
[29] A. Varello, E. Carrera, and L. Demasi, Vortex lattice method coupled with advanced one-dimensional structural models, J. Aeroelast. Struct. Dyn., vol. 2, no. 2, pp. 53–78, 2011. DOI: 10.3293/asdj.2011.10.
[30] A. Varello, A. Lamberti, and E. Carrera, Static aeroelastic response of wing-structures accounting for in-plane cross-section deformation, Int. J. Aeronaut. Space Sci., vol. 14, no. 4, pp. 310–323, 2013. DOI: 10.5139/IJASS.2013.14.4.310.
[31] E. Carrera, A. Varello, and L. Demasi, A refined structural model for static aeroelastic response and divergence of metallic and composite wings, CEAS Aeronaut. J., vol. 4, no. 2, pp. 175–189, 2013. DOI: 10.1007/s13272-013-0063-2.
[32] M. Petrolo, Advanced 1D structural models for flutter analysis of lifting surfaces, Int. J. Aeronaut. Space Sci., vol. 13, no. 2, pp. 199–209, 2012. DOI: 10.5139/IJASS.2012.13.2.199.
[33] M. Petrolo, Flutter analysis of composite lifting surfaces by the 1D Carrera Unified Formulation and the doublet lattice method, Compos. Struct., vol. 95, pp. 539–546, 2013. DOI: 10.1016/j.compstruct.2012.06.021.
[34] A. Pagani, M. Petrolo, and E. Carrera, Flutter analysis by refined 1D dynamic stiffness elements and doublet lattice method, Adv. Aircr. Spacecr. Sci., vol. 1, no. 3, pp. 291–310, 2014. DOI: 10.12989/aas.2014.1.3.291.
[35] E. Carrera and E. Zappino, Aeroelastic analysis of pinched panels in supersonic flow changing with altitude, J. Spacecr. Rockets, vol. 51, no. 1, pp. 187–199, 2014. DOI: 10.2514/1.A32363.
[36] E. Carrera, E. Zappino, K. Patôcka, M. Komarek, A. Ferrarese, M. Montabone, B. Kotzias, B. Huermann, and R. Schwane, Aeroelastic analysis of versatile thermal insulation (VTI) panels with pinched boundary conditions, CEAS Space J., vol. 6, pp. 23–35, 2014. DOI: 10.1007/s12567-013-0054-5.
[37] E. Carrera and M. Filippi, Variable kinematic one-dimensional finite elements for the analysis of rotors made of composite materials, J. Gas Turbo Power, 2014 (In press).
[38] R.L. Bisplinghoff, H. Ashley, and R.L. Halfman, Aeroelasticity, Dover Publications, Inc., Mineola, NY, 1996.
[39] W.P. Rodden, Theoretical and Computational Aeroelasticity, Crest Publishing, Cararillo, CA, 2011.
[40] R. T. Jones, Operational treatment of the non-uniform lift theory in airplane dynamics, Technical Note 667, NASA, 1938.
[41] M. Petrolo, Advanced aeroelastic models for the analysis of lifting surfaces made of composite materials, Ph.D. Dissertation, 2011, Politecnico di Torino, Torino, Italy.
[42] M. Petrolo, Flutter analysis of composite lifting surfaces by the 1D Carrera unified formulation and the doublet lattice method, Compos. Struct., vol. 95, pp. 539–546, 2013. DOI: 10.1016/j.compstruct.2012.06.021.
[43] M. Kameyama and H. Fukunaga, Optimum design of composite plate wings for aeroelastic characteristics using lamination parameters, Comput. Struct., vol. 85, pp. 213–224, 2007. DOI: 10.1016/j.compstruc.2006.08.051.
[44] S.J. Hollowell and J. Dugundji, Aeroelastic flutter and divergence of stiffness coupled, graphite/epoxy cantilevered plates, J. Aircraft, vol. 21, pp. 69–76, 1984. DOI: 10.2514/3.48224.